Grating-Structured Freestanding Triboelectric-Layer Nanogenerator for Harvesting Mechanical Energy at 85% Total Conversion Efficiency

Yannan Xie, Sihong Wang, Simiao Niu, Long Lin, Qingshen Jing, Jin Yang, Zhengyun Wu, and Zhong Lin Wang*

Under the global urgency of the energy crisis and severe environmental problems, an energy harvesting technology that converts ambient energy into electricity has emerged as an important alternative to conventional energy.[1–3] In the past decades, various devices and systems have been rapidly developed based on different types of effects and mechanisms, such as electromagnetic,[4,5] photovoltaic,[6,7] piezoelectric,[8,9] and thermoelectric.[10,11] Targeted at universally-existing mechanical motions, the triboelectric nanogenerator (TENG),[12] based on the conjunction of contact electrification and electrostatic induction,[13–15] has been recognized as one of the most promising approaches. Although the triboelectric effect has been utilized in some devices, such as Van de Graaff generators,[16] TENG has its unique working principle and significant advantages of high efficiency, low cost, reliable robustness, and being environmental friendly.[17] Derived from two basic modes of TENG-the contact mode[18,19] and the sliding mode,[20,21] various device designs have been developed not only for harvesting mechanical energy in different forms (such as water flow and wind power),[22,23] but also for the realization of sustainable power sources through hybridizing with energy storage technologies for self-powered systems.[24–26] Nevertheless, most of the existing TENGs necessitate the attachment of electrodes and lead wires onto moving triboelectric layers, which largely limits the versatile applications of TENGs especially when targeted motions are irregular and from arbitrary objects. Recently, freestanding triboelectric-layer nanogenerator (FTENG), as a new fundamental mode, has been demonstrated to resolve the above issue by making it possible to harvest energy from independent and freely moving targets.[27,28] In such structure, one electrode-free triboelectric layer alternatively approaches two stationary electrodes by sliding motion, resulting in the flow of free electrons across the external load as driven by the periodical change of induced potential difference. With this unique mechanism, the device can even work without direct contact between the triboelectric surfaces, which is called non-contact operation mode. However, this type of device requires a relative large sliding displacement (the whole length of one electrode) to realize an effective electricity generation, which is unfavorable for its achievable power output and energy scavenging in practical use. Since mechanical vibration in our environment is always irregular and varying in amplitude and frequency.

For the improvement in the above two important aspects, we herein report a linear grating-structured freestanding triboelectric-layer nanogenerator (GF-TENG) with largely-elevated output, high efficiency, and broad range of applications. This new design is composed of a grating-segmented triboelectric layer and two pairs of interdigitated electrodes, all in the same periodicity. Both of the theoretical analysis and experimental study indicated significant enhancement in the amount of collectable charges, current density, and output frequency through introducing finer grating segments. As driven by a linear motor at an acceleration of 30 m/s^2, the GF-TENG with 16 grating segments delivered an open circuit voltage (V_{OC}) of ~135 V and a short-circuit current density (J_{SC}) of ~9 mA/m^2, corresponding to a maximum power density of ~1.2 W/m^2. Moreover, we also demonstrated that the device working in non-contact mode (that is free of sliding friction) exhibited supreme stability for a long period and achieved extremely-high total conversion efficiency of 85% at low operation frequency. With these unique features, the GF-TENG was utilized to generate electricity from a wide range of ambient mechanical motion, such as sliding of human hand, acceleration or deceleration of vehicles, and people walking. All these demonstrations reveal a great potential of GF-TENG as a high-efficiency device for practically-applicable mechanical energy harvesting.

The structure of the GF-TENG is depicted in **Figure 1**a. The device mainly consists of two groups of components: a freestanding triboelectric layer with grating segments and two interdigitated metal electrodes. To enable an intensive electrification during contact, fluorinated ethylene propylene (FEP) and Al were chosen as the materials for the freestanding triboelectric layer and metal electrodes, respectively, according to the triboelectric series.[29] In the fabrication of the freestanding part,

Y. Xie,[+] S. Wang,[+] S. Niu,[+] L. Lin, Q. Jing, J. Yang,
Prof. Z. L. Wang
School of Materials Science and Engineering
Georgia Institute of Technology
Atlanta, Georgia 30332–0245, USA
E-mail: zlwang@gatech.edu
Y. Xie, Prof. Z. Wu
Department of Physics
Xiamen University
Xiamen 361005, Fujian, China
Prof. Z. L. Wang
Beijing Institute of Nanoenergy and Nanosystems
Chinese Academy of Sciences
Beijing, China
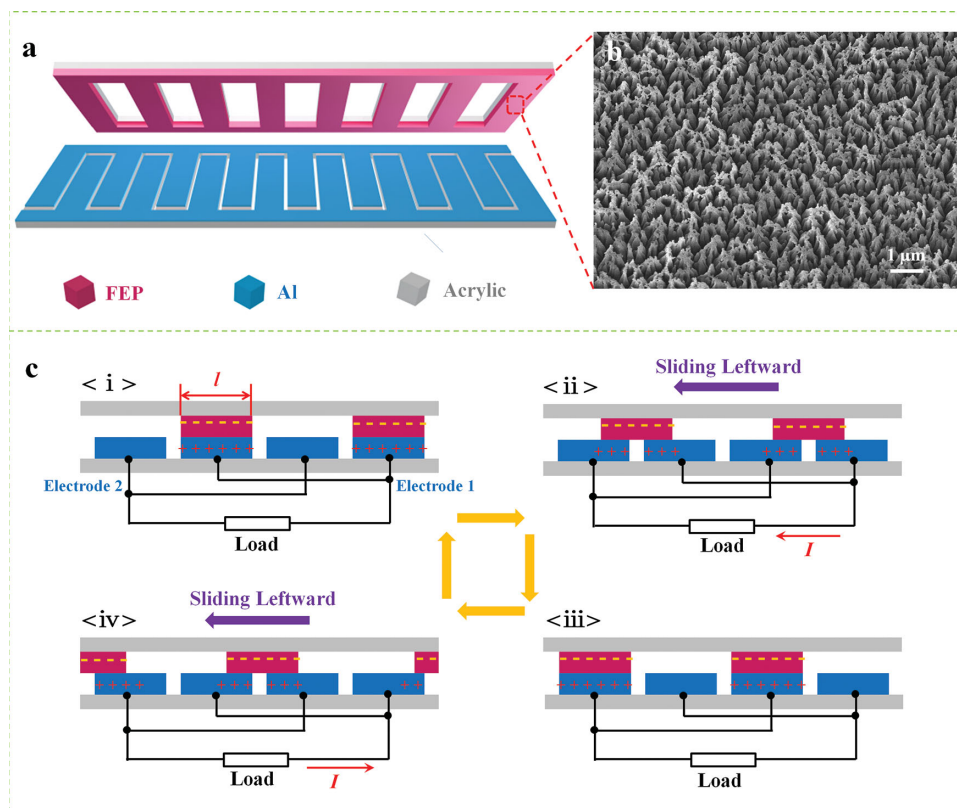[+]These authors contributed equally to this work.

COMMUNICATION

Figure 1. Device structure and operation mechanism of grating-structured freestanding triboelectric-layer nanogenerator (GF-TENG). (a) Typical structure design of GF-TENG. (b) SEM image of nanorod structure on the FEP surface. (c) Working mechanism of the GF-TENG.

an acrylic sheet was laser-cut into grating structures with N segments ($N = 8$ for Figure 1a) as the supporting substrate for the triboelectric layer. Then, the FEP film was adhered to the substrate and cut into the same configuration. To enhance the contact electrification, nanorod structures (Figure 1b) was introduced onto the surface of FEP film through inductive coupling plasma reactive ion etching.[19,30] As for the metal-electrode part, another acrylic was patterned to N units of interdigitated structures with the same periodicity as the freestanding layer. After the deposition of aluminum film, two groups of grated-electrodes with the complimentary shape were obtained. The spacing between two adjacent electrode fingers was 1 mm in all the devices. For the GF-TENGs with different N, we maintained the total effective lengths (l_0) of the freestanding layer and each electrode group with the same value of 6.4 cm, which makes sure these devices having the same total effective area (38.4 cm^2). Thus, the larger number of segments only brings about the smaller length (l) of each grating unit, with a relationship of $l = l_0/N$.

The operation principle of the GF-TENG can be explained as the coupling of contact electrification and in-plane-sliding-induced charge transfer, as shown in Figure 1c. Initially, the grating rows of the FEP layer are brought into contact with the fingers of the electrode group (EG) 1 at a fully overlapping position (Figure 1c<i>). Since FEP is more triboelectrically negative than Al, contact electrification between two surfaces occurs, which results in negative charges on the FEP surface and positive charges on the EG 1 with the equal amount.[31,32]

In this state, there is no charge flowing between the two electrodes due to the electrostatic equilibrium. When the FEP layer starts to slide leftward, this grated layer gradually moves from the overlapping position of EG 1 to that of EG 2 (Figure 1c<ii>). In this case, an electric potential drop is generated and drives positive charges flow from the EG 1 to the EG 2 along with the sliding motion, which produces a transient current in the external load. Once the FEP layer reaches the fully overlapping position with EG 2 (Figure 1c<iii>), all of the positive charges transfer to this electrode, with another electrostatic equilibrium being achieved. This is one unit step of sliding. When the FEP continues to slide leftward to the EG 1 by another step (Figure 1c<iv>), the positive charges will be electrostatically attracted to flow back to EG 1, bringing about a reverse current in the circuit. Therefore, an electricity generation cycle is completed. If the FEP is driven to slide rightward, a reverse process will take place.

To theoretically investigate the influence of introducing grating segments on the electrical characteristics of the GF-TENGs, we employed finite element method to simulate the open-circuit voltage (V_{OC}) and short-circuit transferred charge density ($\Delta\sigma_{SC}$) of two structures with the same effective area but different number of segmentations N ($N = 1$ and 4, respectively) through COMSOL software. The simulation covers the entire unidirectional sliding process that starts off from the position that FEP fully overlaps with EG 1 (**Figure 2**a<i>) to the end position that only one grating segment of FEP overlaps with one electrode finger of EG 2 (Figure 2a<ii>). Therefore,

Materials
Views
www.MaterialsViews.com

ADVANCED
MATERIALS
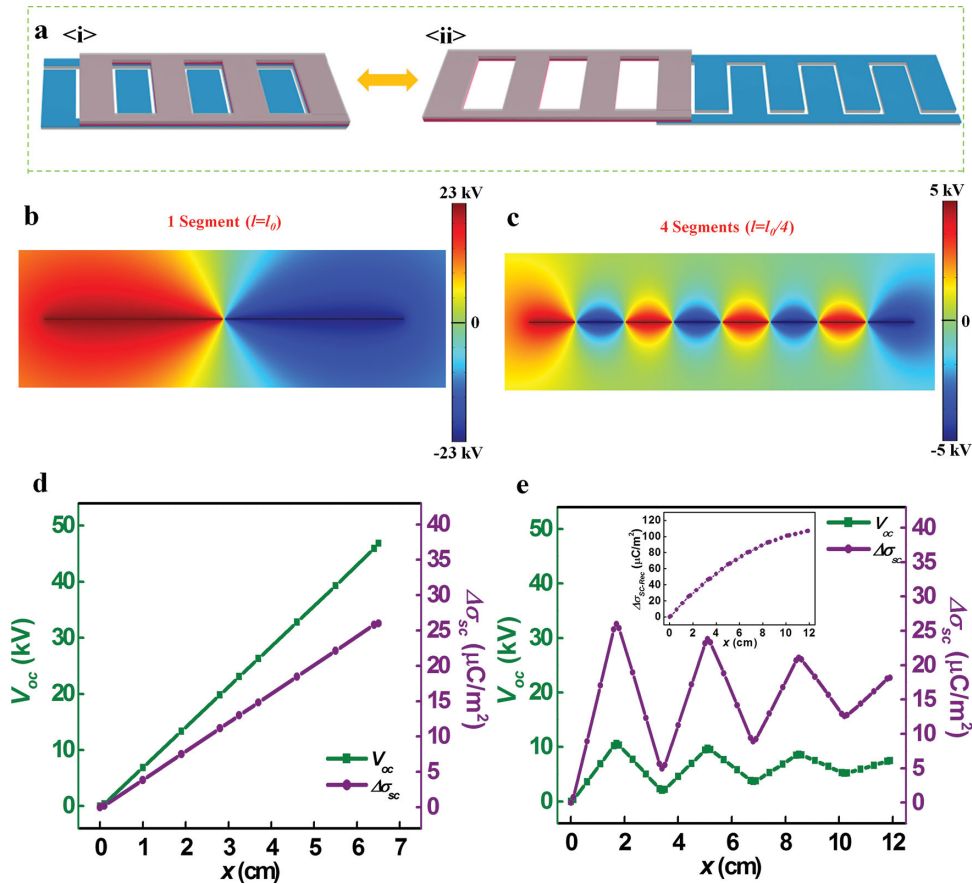www.advmat.de

COMMUNICATION

Figure 2. Theoretical model and study of GF-TENGs. (a) The initial and final states of one-way sliding. (b) The simulated potential distributions after one step of sliding for the GF-TENG with 1 segment. (c) The simulated potential distributions after one step of sliding for the GF-TENG with 4 segments. (d) The simulated open-circuit voltages (V_{OC}) and transferred charge densities ($\Delta\sigma_{SC}$) at different sliding displacements (x) for the GF-TENG with 1 segment. (e) The simulated V_{OC} and $\Delta\sigma_{SC}$ at different sliding displacements for the GF-TENG with 4 segments, the inset is the result of rectified transferred charge density ($\Delta\sigma_{SC-Rec}$).

there will be (2N-1) unit steps in a one-way sliding process for the GF-TENG with N segments. Initially, a tribo-charge density of 26 μC/m^2 (which was chosen based on the measured result) was assigned for both of the structures: a uniform distribution of negative charges on the FEP layer and positive charges on the EG 1. One unit step of sliding brings the FEP layer to the position of EG 2. The lateral separation of the opposite charges in the open-circuit condition will induce an electrical potential difference (V_{OC}) between EG 1 and EG 2. As shown in Figure 2b-c, the fingers in EG 1 are in positive potential while the EG 2 fingers are all in negative potential. Figure 2d-e shows the quantitative relationship of V_{OC} and $\Delta\sigma_{SC}$ with the displacement (x) in a one-way sliding process. After one unit step (x = 6.5 and 1.7 cm for N = 1 and 4, respectively), high potential differences are generated for both of the two structures with the same transferred charge density ($\Delta\sigma_{SC}$ = 26 μC/m^2) from EG 1 to EG. It is noted that the simulated V_{OC} of 1 segment device is ~46 kV, which is much higher than that (~10 kV) of 4 segments device. The result can be explained by the general relationship between V_{OC} and $\Delta\sigma_{SC}$ in TENG[33,34]:

$$V_{OC} = \frac{\Delta\sigma_{SC} \cdot S}{C} \qquad (1)$$

where S is the total area of electrode 1 or electrode 2, and C is the capacitance between electrode 1 and electrode 2. Considering that $\Delta\sigma_{SC}$ and S are keeping constant and that dividing electrodes into smaller segments will increases C,[33] consequently, the device with more grating segments corresponds to a lower V_{OC}. For the 1 segment device, since there is only one sliding step in the structure, the tribo-charges are transferred once within the whole procedure (x = 6.5 cm), as indicated by the monotonic curves in the figure. When it comes to the GF-TENG with 4 segments, both of the V_{OC} and $\Delta\sigma_{SC}$ oscillate seven times with obvious decaying tendencies in the whole process (x = 11.9 cm), corresponding to seven steps of sliding with the total contact area declining. If the device is connected to a bridge rectifier, the transferred charges can be accumulated and the rectified transferred charge density ($\Delta\sigma_{SC-Rec}$) shows a rising trend with the x, rather than an oscillation behavior, which can be observed in the inset of Figure 2e. After the one-way sliding, the $\Delta\sigma_{SC-Rec}$ reaches as high as 106 μC/m^2, which is over four times larger than that (26 μC/m^2) of one segment device. Based on the above discussion, we can make some conclusions as follows: if a GF-TENG has N segments in structure, (1) both of the V_{OC} and $\Delta\sigma_{SC}$ will oscillate (2N-1) times within a one-way sliding process, corresponding to (2N-1) times of charge
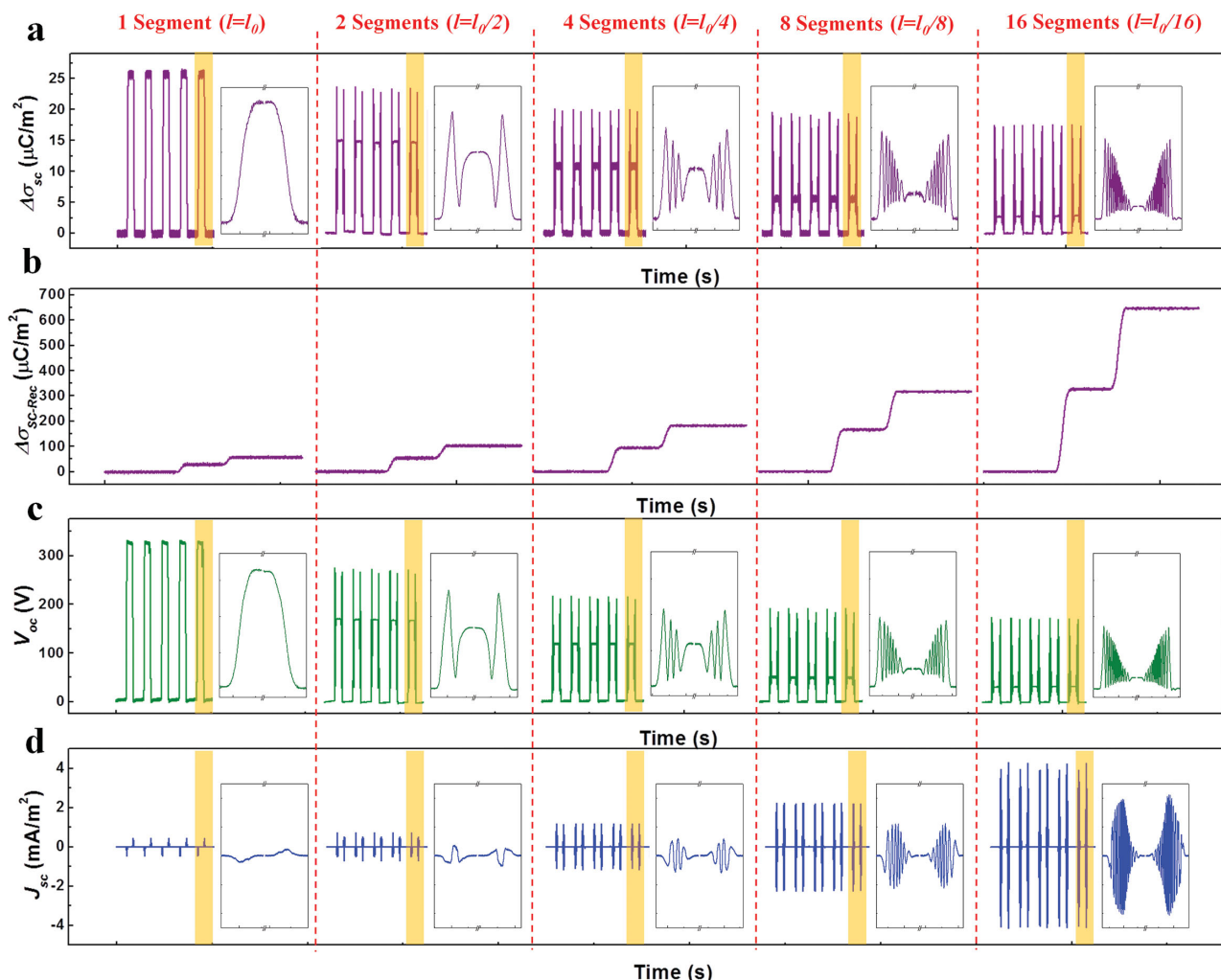
Figure 3. Electrical measurement results of GF-TENGs with different segment strucutres ($N = 1, 2, 4, 8, 16$). (a) The measured $\Delta\sigma_{SC}$. (b) The measured $\Delta\sigma_{SC\text{-}Rec}$. (c) The measured V_{OC}. (d) The measured short-circuit current density (J_{SC}). The insets show the enlargement of the corresponding highlighted parts.

transfer; (2) the V_{OC} will decrease with the increase of N; (3) the $\Delta\sigma_{SC\text{-}Rec}$ will increase with the increase of N.

To experimentally study the influence of the grating segmentations on the output performance, five devices with different grating segments ($N = 1, 2, 4, 8, 16$) but the same effective area were fabricated, and their electrical characteristics were measured. The V_{OC}, $\Delta\sigma_{SC}$, and $\Delta\sigma_{SC\text{-}Rec}$ were measured by Keithley 6514 system, and the short-circuit current density (J_{SC}) was measured by SR570 low noise current amplifier (Stanford Research System). **Figure 3**a shows the transferred charge density of the GF-TENGs with insets showing the enlargement profiles of one sliding cycle of each structure. A full sliding cycle is composed of two parts with the left part corresponding to a one-way sliding and the right one representing the backward process. It can be observed that tribo-charges are transferred ($2N-1$) times for the N segments device (e.g., 31 times for 16 segments) in a one-way process, which is accordant with the simulation work, although the maximum $\Delta\sigma_{SC}$ from the first step declines slightly with the increase of N. The trends may be ascribed to the uneven surface induced by the procedure

of laser cutting of grating structure, which affects the effective contact area. By connecting the GF-TENGs with a bridge rectifier, all of the transferred charges can be accumulatively collected, e.g. in an energy storage device. As shown in Figure 3b, the accumulated charges have a largely-enhanced amount by increasing segment numbers because of multiplied charge transfer cycles. When 16 segments are introduced, the $\Delta\sigma_{SC\text{-}Rec}$ goes up to 640 µC/m² which is over 10 times larger than that of 1 segment structure, demonstrating a huge enhancement in performance for the multiple segmentation structured device. As for the V_{OC}, the profiles display similar oscillation behaviors as the $\Delta\sigma_{SC}$ with a much more severe decaying tendency by the increase of N. This reflects the prediction in the theoretical analysis. The characteristics of the J_{SC} were shown in Figure 3d, which were measured at a sliding acceleration of 10 m/s². For 1 segment device, only one low and wide current peak was generated by one unidirectional sliding step; when it comes to 16 segments structure, 31 sharp and narrow peaks are produced with a peak value of ~4.0 mA/m² from a similar one-way sliding step. The mean frequencies of the two GF-TENGs are

Materials
Views
www.MaterialsViews.com

ADVANCED
MATERIALS
www.advmat.de

COMMUNICATION

about 7 and 130 Hz, respectively. The enhanced performance can be explained by the following equation[20,33]:

$$J_{SC} = \frac{d\Delta\sigma_{SC}}{dt} \qquad (2)$$

where t is the time. Since both of the length and the time for each unit step will be shorter when the segmentation number increases, tribo-charges can be transferred faster and hence the higher amplitude and frequency are achieved for the current. Therefore, introducing more grating segments in the structure will be favorable for the accumulation of charges, current density and frequency.

In the above case where the FEP layer and the electrode groups have the same number of units, the total effective area decreases while the FEP slides outwards, resulting in a damped oscillation behavior of $\Delta\sigma_{SC}$. In order to make the electricity generation more effective through maintaining the same effective area during the sliding of FEP, we fabricated an extended GF-TENG in which electrode part has the doubled number of units compared with the FEP layer. In this design, the FEP will always slides within the range of the electrodes (**Figure 4**a). Figure 4b-e present the output performance of the extended GF-TENG with 16 grating segments. It can be observed that each unit step of sliding transfers almost the same amount

of charges ($\Delta\sigma_{SC} = 16.5 \mu C/m^2$) between the two electrodes without any decay during an entire unidirectional sliding process (Figure 4b). If these transferred charges are accumulated, $\Delta\sigma_{SC-Rec}$ can reach 1100 $\mu C/m^2$ in the process (Figure 4c), which is nearly twice as large as that from the previous non-extended structure. A similar undamped oscillation behavior is observed for V_{OC}, although the amplitude (135 V) becomes smaller than the original one (Figure 4d). The decrease can be ascribed to the increase of the total capacitance between two electrodes from the doubled number of electrode fingers, according to the Equation (1). As for the current, when the acceleration is kept at 10 m/s², the peak value of J_{SC} increases to 5.5 mA/m² due to the enhanced amount of the transferred charges. When the sliding movement has a larger speed, the magnitude of J_{SC} will be further increased, as illustrated in Figure S1. As a power source in practical use, the TENG will be connected with external loads. Therefore, the actual voltages and current densities on varied load resistances were measured and the results are summarized in Figure 4f. The current density (at the acceleration of 30 m/s²) drops at larger external resistances, while the voltage across the load exhibits a reversed tendency. Accordingly, the power density that the device provides firstly rises at low resistance region and then declines at high resistance, showing a maximum value of 0.72 W/m² at the load resistance of 5 MΩ (Figure 4g).
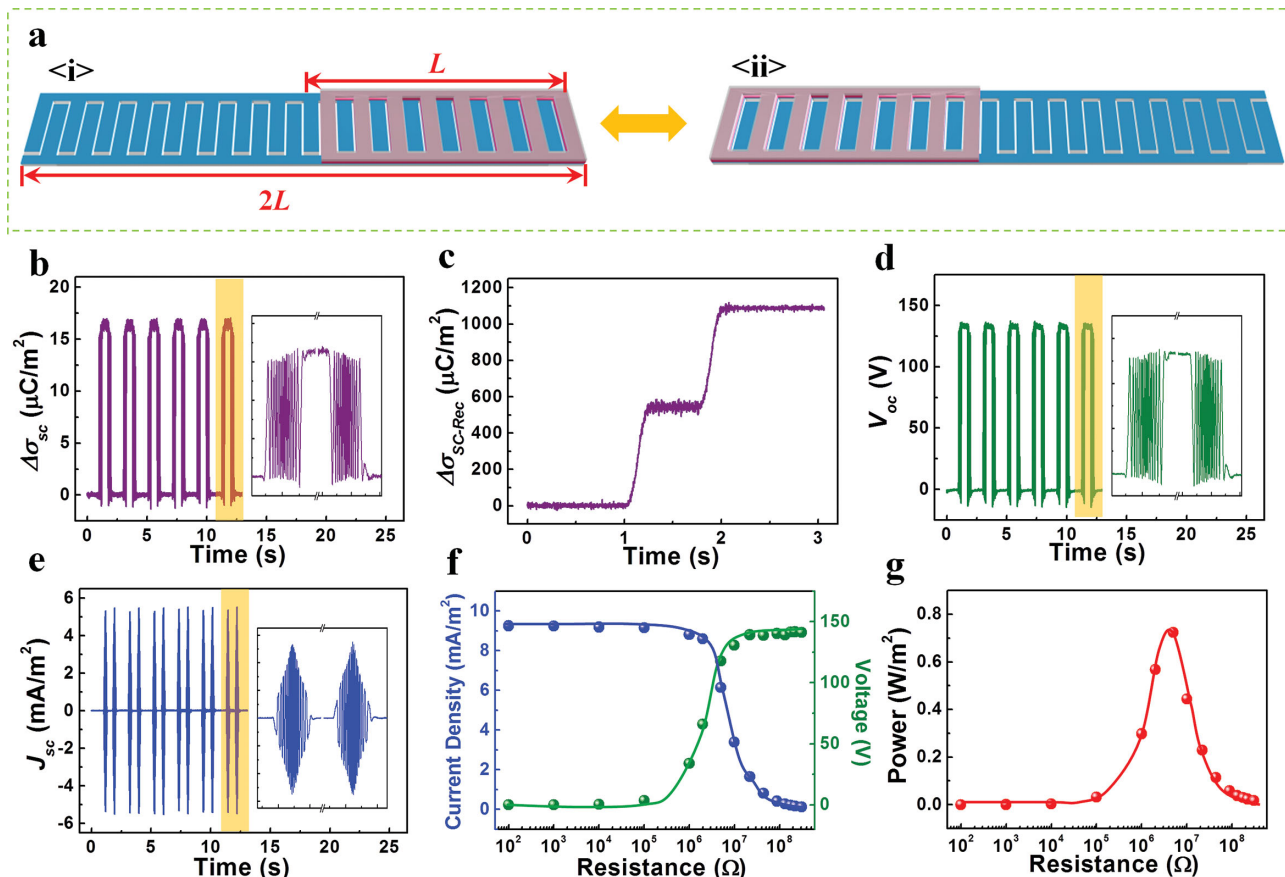

Figure 4. Electrical measurement results of the extended GF-TENGs. (a) The initial and final states of one-way sliding for a typical extended GF-TENG. (b–g) The measured results for the extended GF-TENG with 16 segments: (b) The $\Delta\sigma_{SC}$; (c) The $\Delta\sigma_{SC-Rec}$; (d) The V_{OC}; (e) The J_{SC}; (f) The dependence of the output voltage, current density, and (g) power density on the resistance of the external load.
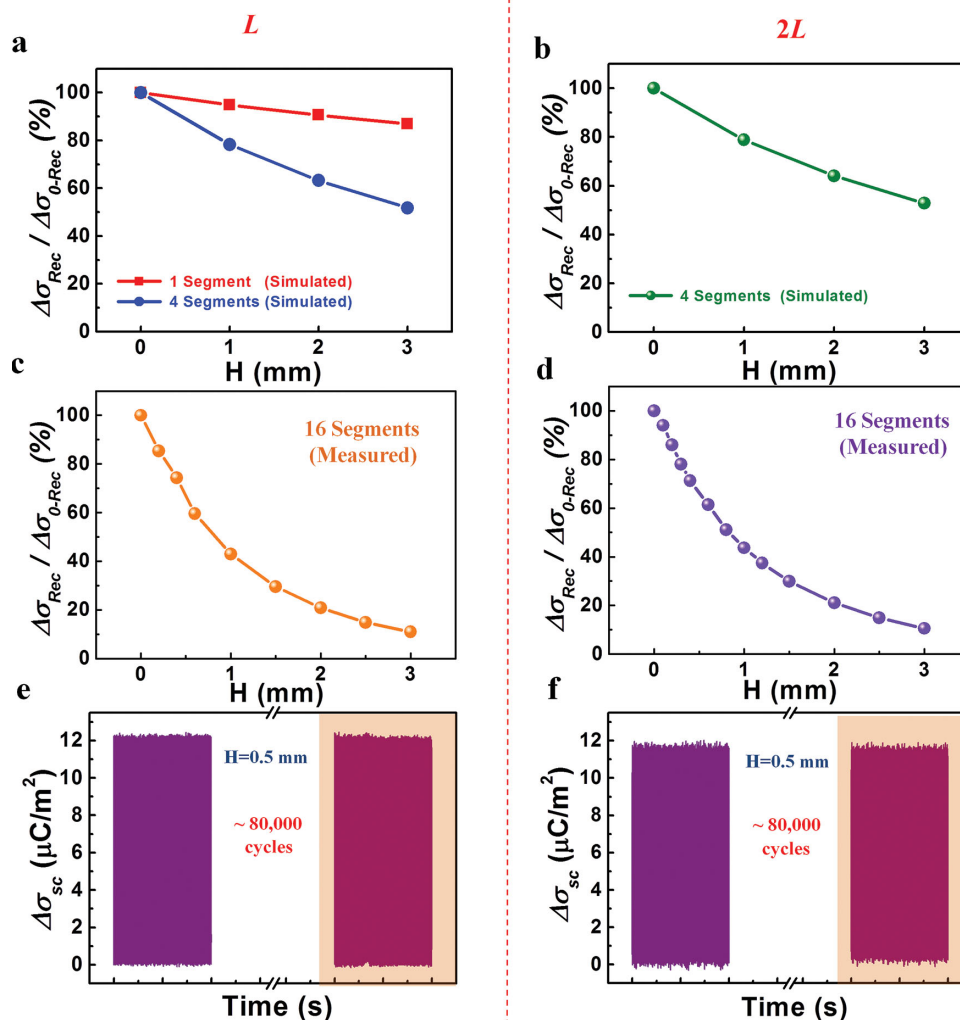
Figure 5. Theoretical and experimental investigations on GF-TENGs working in non-contact mode. (a) The simulated results about the influence of vertical gap (H) on accumulated transferred charge densities ($\Delta\sigma_{Rec}$) for GF-TENGs with 1 segment and 4 segments. (b) The simulated results about the influence of H on $\Delta\sigma_{Rec}$ for the extended GF-TENG with 4 segments. (c) The measured results about the influence of H on $\Delta\sigma_{Rec}$ for the GF-TENG with 16 segments. (d) The measured results about the influence of H on $\Delta\sigma_{Rec}$ for the extended GF-TENG with 16 segments. (e) The output stability of the GF-TENG with 16 segments working in non-contact mode. (f) The output stability of the extended GF-TENG with 16 segments working in non-contact mode.

Besides the contact sliding working condition as discussed above, the GF-TENGs can also be operated in non-contact situation with an air gap existing between the FEP and the electrodes plane, which is a unique feature of FTENGs compared with any other types of TENGs.[27,28] To obtain a comprehensive understanding about this operation mode of GF-TENG, we theoretically investigate the influence of the vertical gap distance (H) on the amount of transferred charges. **Figure 5**a shows the simulation results of the non-extended devices that are discussed in the Figure 2. As can be observed, when H is increased from 0 to 3 mm, the accumulated transferred charge densities ($\Delta\sigma_{Rec}$) in one sliding cycle decline to certain percentages of the original value at $H = 0$ ($\Delta\sigma_{0-Rec}$): 87% for 1 segment device and 52% for 4 segments device, which means the influence of the vertical separation will be a bit more severe when segmentation

number is increased. However, it needs to be pointed out that $\Delta\sigma_{0-Rec}$ of 4 segments structure is over four times larger than that of 1 segment structure. Therefore, the GF-TENG with 4 segments can produce a larger charge output within a smaller displacement even at $H = 3$ mm, showing large enhancement of charge transfer efficiency. For the extended GF-TENG with 4 grating segments, the decaying rate of $\Delta\sigma_{Rec}$ almost keeps unchanged compared to the non-extended device (Figure 5b). Figure 5c–d show experimental results of the 16 segments GF-TENGs without and with being extended (L and $2L$), respectively. The changing behaviors of the two devices are nearly the same with each other: decreasing gradually to ~11% while H is raised to 3 mm. The non-contact working mode will give rise to supreme stability for the GF-TENGs. As shown in Figure 5e–f, when the devices are operated continuously for 80 000 cycles at

Materials
Views
www.MaterialsViews.com

ADVANCED
MATERIALS
www.advmat.de

COMMUNICATION

a gap distance of 0.5 mm, both of the devices display little decay in the output performance. Such excellent stability is attributed to two aspects: (1) FEP, the freestanding triboelectric layer, is a type of electret which can quasi-permanently retain the static charges on them for a long time;[31,35] (2) there is no abrasion on the tribo-charged surfaces during the non-contact operation; therefore the life time of the devices can be prolonged to a large extent.

With the unique advantages as demonstrated above, the GF-TENGs can be employed to harvest numerous kinds of mechanical energy existing in our environment and act as direct power sources for electronics. As shown in **Figure 6**a and Video S1, after attaching a freestanding FEP film to a human hand, the hand can slide freely across the electrodes without any constrain. This movement can effectively generate electricity to light up 60 commercial LEDs (Nichia NSPG500DS) instantaneously even under a slow speed and a small displacement. The GF-TENG can also be potentially utilized to harvest the vibration energies from moving vehicles. For the demonstration, a GF-TENG is installed to a remote control car. When the car was in the acceleration or deceleration, the GF-TENG can generate electricity for powering electronic components on the vehicle (Figure 6b and Video S2). The GF-TENG could also be used as a self-powered sensor for detecting the acceleration of moving vehicles. If the generator is fully sealed, it can be further applied to harvest wave/tidal energy from the sea.

Furthermore, the GF-TENG working in non-contact mode can harvest mechanical energy with high conversion efficiency. As shown in Figure 6c, four identical extension springs (McMaster-Carr 9654K511) are used to position the FEP within the parallel plane to the surface of the electrodes with a distance of 1.6 mm. When the external mechanical motion applies onto the device along the spring direction, the FEP will oscillate around the equilibrium position for a long term without extra mechanical input, converting the stored mechanical energy in the spring into electricity. As shown in Figure 6d and Video S3, this design can scavenge the mechanical energy from people's walking motion when it is bonded to human legs. It is noticed that each walking step will produce lasting and decaying electrical outputs in a certain period, which corresponds to the damped oscillation of the FEP around the equilibrium position.
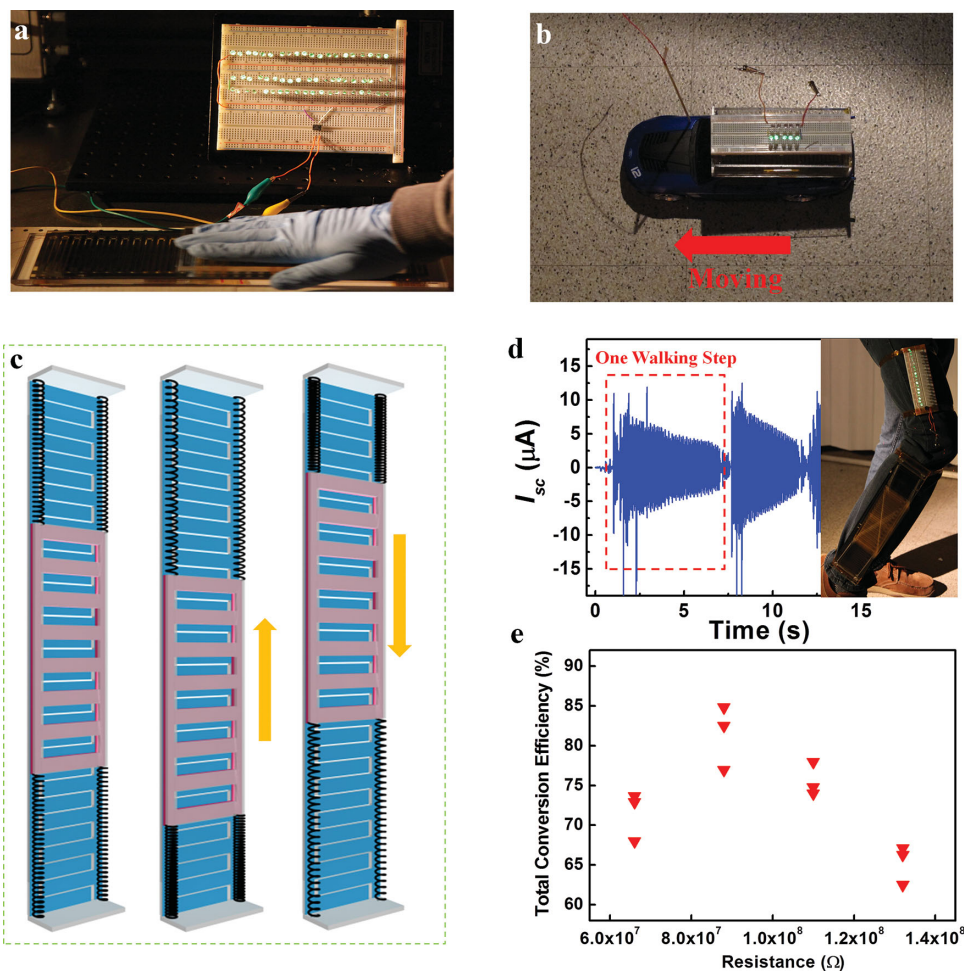

Figure 6. Applications of GF-TENG for harvesting a wide range of mechanical energy. (a) Harvesting energy from sliding of a human hand. (b) Harvesting energy from acceleration or deceleration of a remote control car. (c) Device structure for non-contact GF-TENG. (d) Harvesting energy from people walking by non-contact GF-TENG and the real-time measurement of short-circuit current (I_{sc}). (e) Total conversion efficiency of non-contact GF-TENG for harvesting slight vibration under different load resistances.

COMMUNICATION

This spring-based device can also be utilized to estimate the conversion efficiency of the GF-TENG in non-contact mode. Here, total conversion efficiency is introduced and defined as the ratio of the total generated electrical power (by the instantaneous triggering and the residual mechanical vibration after the triggering) to the input mechanical power. Ideally, if there is not any friction in the environment, the theoretical total conversion efficiency of non-contact mode is expected to be 100%. However, in the real situation, air friction, a non-neglectable factor, will bring about an energy loss for the device working against it. To reduce the impact of air resistance, we can make the FEP oscillate at a low speed (slight vibration). Therefore, high total conversion efficiency would be achieved in this situation. During the measurement, the FEP is initially pulled to a position with a small displacement ($x = 1$ mm) relative to the equilibrium point, through which the mechanical energy is stored in the springs. When the FEP layer is released at this point, it will oscillate around the equilibrium position with gradually damping amplitude for ~4 min. In this process, the stored mechanical energy is gradually converted firstly to kinetic energy of the FEP and then to the electrical energy. Through measuring the electrical output on the external load, the total amount of electrical energy can be calculated. Similar to the power measurement in Figure 4g, the electrical energy obtained by the load reaches the maximum values at a certain resistance. Thus, we measured the current on a series of loads with different resistances in order to get the highest-achievable electrical energy and hence the efficiency. Therefore, the total generated electrical power can be calculated as:

$$E_{electrical} = \int I^2 \cdot R \cdot dt \qquad (3)$$

where I is the instantaneous current which can be recorded by electrometer, R is the load resistance. Figure S2 shows the highest electrical energy generated during the measurement process. As for the input mechanical energy, it will be determined by the difference between potential energy at initial position ($x = 1$ mm) and final position (equilibrium point), which can be calculated as (supporting information):

$$E_{mechanical} = 2 \cdot k \cdot x^2 \qquad (4)$$

where k is the spring constant of a single spring ($k = 15.76$ N/m), x is its displacement ($x = 1$ mm). Figure 6e shows the estimated total conversion efficiency under different resistances from a number of repeated measurements. It can be observed that the highest efficiency reaches 85% at an external load of 88 MΩ. It clearly demonstrates the capability of harvesting mechanical energy at a very high efficiency by the freestanding-layer-mode triboelectric nanogenerator. It is worth noting that the optimum resistance in the efficiency measurement is higher than that (5 MΩ) in the Figure 4g. The reason is that these two measurements are operated at different sliding velocities which will largely change the frequency characteristic of the device and hence the optimum resistance. In practical application, to achieve the impedance match between the nanogenerator and the external load, power management can be employed to form a complete power-supplying system.

In summary, we have demonstrated a new design of a triboelectric nanogenerator, which consists of a freestanding triboelectric-layer with grating segments and two stationary electrodes with interdigitated patterns. With grating units that sweep across the electrode fingers, multiple alternating currents are generated between the two electrodes due to electrostatic induction in both contact and non-contact mode. According to the theoretical and experimental investigation, the GF-TENG with finer grating units exhibits improved performance in terms of the amount of collectable charges, current density, and output frequency. When the device is operated in non-contact mode, it shows an excellent stability and high total conversion efficiency up to 85% at low operation frequency. On the basis of these advantages, the GF-TENG is capable of harvesting energy from a variety of ambient sources, such as sliding of human hand, acceleration of vehicles, and people walking. This work represents a significant progress of TENG and exhibits huge potential of the GF-TENG as a high-efficiency energy harvester for practical applications.

Supporting Information

Supporting Information is available from the Wiley Online Library or from the author.

Acknowledgements

[1] N. Armaroli, V. Balzani, *Angew. Chem.-Int. Edit.* **2007**, *46*, 52.
[2] Z. L. Wang, *Adv. Funct. Mater.* **2008**, *18*, 3553.
[3] N. L. Panwar, S. C. Kaushik, S. Kothari, *Renew. Sust. Energ. Rev.* **2011**, *15*, 1513.
[4] S. P. Beeby, R. N. Torah, M. J. Tudor, P. Glynne-Jones, T. O'Donnell, C. R. Saha, S. Roy, *J. Micromech. Microeng.* **2007**, *17*, 1257.
[5] I. Sari, T. Balkan, H. Kulah, *Sensor Actuat. a-Phys.* **2008**, *145*, 405.
[6] W. U. Huynh, J. J. Dittmer, A. P. Alivisatos, *Science* **2002**, *295*, 2425.
[7] B. Z. Tian, X. L. Zheng, T. J. Kempa, Y. Fang, N. F. Yu, G. H. Yu, J. L. Huang, C. M. Lieber, *Nature* **2007**, *449*, 885-U8.
[8] Z. L. Wang, J. H. Song, *Science* **2006**, *312*, 242.
[9] C. E. Chang, V. H. Tran, J. B. Wang, Y. K. Fuh, L. W. Lin, *Nano Lett.* **2010**, *10*, 726.
[10] T. Cole, *Science* **1983**, *221*, 915.
[11] D. Kraemer, B. Poudel, H. P. Feng, J. C. Caylor, B. Yu, X. Yan, Y. Ma, X. W. Wang, D. Z. Wang, A. Muto, K. McEnaney, M. Chiesa, Z. F. Ren, G. Chen, *Nat. Mater.* **2011**, *10*, 532.

Materials
Views

www.MaterialsViews.com

ADVANCED
MATERIALS
www.advmat.de

COMMUNICATION

[12] F. R. Fan, Z. Q. Tian, Z. L. Wang, *Nano Energy* **2012**, *1*, 328.

[13] G. Zhu, C. F. Pan, W. X. Guo, C. Y. Chen, Y. S. Zhou, R. M. Yu, Z. L. Wang, *Nano Lett* **2012**, *12*, 4960.

[14] B. A. Grzybowski, A. Winkleman, J. A. Wiles, Y. Brumer, G. M. Whitesides, *Nat. Mater.* **2003**, *2*, 241.

[15] H. T. Baytekin, A. Z. Patashinski, M. Branicki, B. Baytekin, S. Soh, B. A. Grzybowski, *Science* **2011**, *333*, 308.

[16] R. J. Van de Graaff, *Electrostatic generator.* U.S. Patent *1,991,236*, Feb. 12, **1935**.

[17] Z. L. Wang, *ACS Nano* **2013**, *7*, 9533.

[18] S. H. Wang, L. Lin, Z. L. Wang, *Nano Lett.* **2012**, *12*, 6339.

[19] G. Zhu, Z. H. Lin, Q. S. Jing, P. Bai, C. F. Pan, Y. Yang, Y. S. Zhou, Z. L. Wang, *Nano Lett.* **2013**, *13*, 847.

[20] S. H. Wang, L. Lin, Y. N. Xie, Q. S. Jing, S. M. Niu, Z. L. Wang, *Nano Lett.* **2013**, *13*, 2226.

[21] G. Zhu, J. Chen, Y. Liu, P. Bai, Y. S. Zhou, Q. S. Jing, C. F. Pan, Z. L. Wang, *Nano Lett.* **2013**, *13*, 2282.

[22] Z. H. Lin, G. Cheng, L. Lin, S. Lee, Z. L. Wang, *Angew. Chem.-Int. Edit.* **2013**, *52*, 12545.

[23] Y. N. Xie, S. H. Wang, L. Lin, Q. S. Jing, Z. H. Lin, S. M. Niu, Z. Y. Wu, Z. L. Wang, *ACS Nano* **2013**, *7*, 7119.

[24] S. H. Wang, Z. H. Lin, S. M. Niu, L. Lin, Y. N. Xie, K. C. Pradel, Z. L. Wang, *ACS Nano* **2013**, *7*, 11263.

[25] L. Lin, Y. N. Xie, S. H. Wang, W. Z. Wu, S. M. Niu, X. N. Wen, Z. L. Wang, *ACS Nano* **2013**, *7*, 8266.

[26] X. S. Zhang, M. D. Han, R. X. Wang, F. Y. Zhu, Z. H. Li, W. Wang, H. X. Zhang, *Nano Lett* **2013**, *13*, 1168.

[27] S. H. Wang, Y. N. Xie, S. M. Niu, L. Lin, Z. L. Wang, *Adv. Mater.* **2014**, DOI: 10.1002/adma.201305303.

[28] L. Lin, S. H. Wang, S. M. Niu, C. Liu, Y. N. Xie, Z. L. Wang, *ACS Appl. Mater. Interfaces* **2014**, *6*, 3031.

[29] A. F. Diaz, R. M. Felix-Navarro, *J. Electrostat.* **2004**, *62*, 277.

[30] H. Fang, W. Z. Wu, J. H. Song, Z. L. Wang, *J. Phys. Chem. C* **2009**, *113*, 16571.

[31] L. S. McCarty, G. M. Whitesides, *Angew. Chem. Int. Edit.* **2008**, *47*, 2188.

[32] L. H. Lee, *J. Electrost.* **1994**, *32*, 1.

[33] S. M. Niu, Y. Liu, S. H. Wang, L. Lin, Y. S. Zhou, Y. F. Hu, Z. L. Wang, *Adv. Mater.* **2013**, *25*, 6184.

[34] S. M. Niu, S. H. Wang, L. Lin, Y. Liu, Y. S. Zhou, Y. F. Hu, Z. L. Wang, *Energy Environ. Sci.* **2013**, *6*, 3576.

[35] G. M. Sessler, J. Hillenbrand, *Appl. Phys. Lett.* **1999**, *75*, 3405.